THEORETICAL BOUNDS ON PARALLEL IMAGING IMPLICIT DATA CRIMES IN AN MRI REPRODUCING KERNEL HILBERT SPACE

Evan Frenklak¹, Yamin Arefeen^{1,2}, and Jonathan I Tamir¹

¹Chandra Family Department of Electrical and Computer Engineering, UT Austin, TX, United States ²MD Anderson Cancer Center, Houston, TX, United States

ABSTRACT

Magnetic Resonance Imaging (MRI) diagnoses and manages a wide range of diseases, yet long scan times drive high costs and limit accessibility. AI methods have demonstrated substantial potential for reducing scan times, but despite rapid progress, clinical translation of AI often fails. One particular class of failure modes, referred to as implicit data crimes, are a result of hidden biases introduced when MRI datasets incompletely model the MRI physics of the acquisition. Previous work identified data crimes resulting from algorithmic completion of k-space with parallel imaging and drew on simulation to demonstrate the resulting downstream biases. This work proposes a mathematical framework to re-characterize the problem as one of error reduction during interpolation between sets of evaluation coordinates. We establish a generalized matrix-based definition of the reconstruction error upper bound as a function of the input sampling pattern. Experiments on relevant sampling pattern structures demonstrate the relevance of the framework and suggest future directions for analysis of data crimes.

Index Terms— MRI, implicit data crimes, parallel imaging, reproducing kernel Hilbert spaces

1. INTRODUCTION

Magnetic Resonance Imaging (MRI) is critical for the diagnosis and assessment of wide ranging diseases and anatomy, but long scan time substantially raises costs and precludes equitable access [1]. Artificial intelligence (AI) methods have substantively demonstrated potential for reducing scan times [2], but robust clinical translation of AI remains challenging, both in general healthcare [3] and accelerated MRI reconstruction. For example, studies have shown that AI reconstruction methods achieve excellent quantitative performance but frequently distort or erase small, critical features [4] and that the pipeline of training by retrospectively sub-sampling k-space data potentially makes the model unreliable on realistic clinical data [5].

Implicit data crimes have been identified as a critical barrier to the robust clinical deployment of AI for accelerated MRI reconstruction [6]. Open datasets facilitate community wide development of AI, yet many datasets do not contain true raw k-space data, but rather contain processed data that subtly alter the underlying signal statistics. Thus, models trained on such data may perform well in retrospective benchmarks, as processing like zero-padding or JPEG compression reduce data entropy [6], but will degrade on real clinical data.

A recent study identified a new data crime from the observation that most clinical acquisitions measure k-space with subsampling due to the proliferation of multi-coil receive arrays and parallel imaging (PI) [7]. As a result, curation of data repositories from these clinical acquisitions first involves reconstructing the data with PI. Although these data appear fully-sampled, previous work empirically demonstrated that reconstruction methods evaluated on these algorithmically completed data degrade on realistic, prospective sub-sampled data [8]. Figure 1 conceptually describes this data crime and Figure 2 shows an example of this PI algorithmic completion in a popular public MRI dataset.

In this work, we propose a novel theoretical framework to fully characterize the data crime of evaluating reconstructions on PI-completed data. We extend theory framing PI as linear interpolation in a reproducing-kernel-hilbert-space (RKHS) [9] by modeling the crime as a two-stage re-sampling process in k-space. From this, we derive reconstruction operators and analytical error bounds corresponding to the two-stage re-sampling process allowing for theoretical characterization and evaluation of the crime. Crucially, our results are data-independent and only rely on the sampling points themselves.

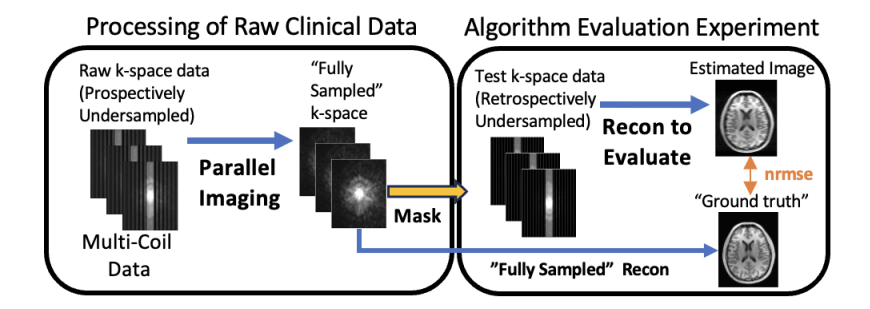


Fig. 1: Conceptual framework for the implicit data crime: Prospective sub-sampling occurs in clinical scanner settings. PI fills in missing k-space data before it is presented as a "fully sampled" dataset. Retrospectively sub-sampling the algorithmically completed data and comparing it to the PI reconstructed data leads to biased performance evaluation.

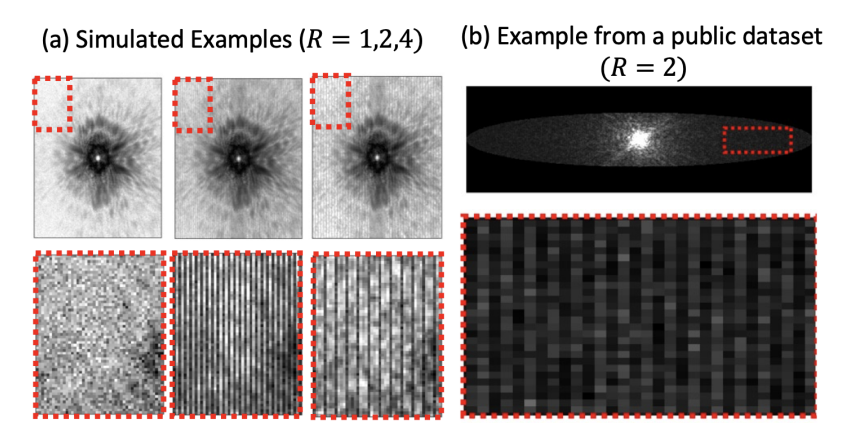


Fig. 2: (a) Simulated examples of PI completed k-space and (b) an example k-space completed by PI on a public dataset. Stripes are present in the log-magnitude k-space images because some points have been algorithmically synthesized.

2. THEORY

2.1. RKHS-based MRI Reconstruction

Figure 3 shows the theoretical and computational framework. Existing theory [9] frames PI as linear interpolation in a RKHS, where sampling at k-space point \mathbf{y} is described by the inner product $f_j(\mathbf{y}) = \langle \epsilon_j^{\mathbf{y}}, \rho \rangle$ between the continuous image, $\rho(\mathbf{r})$, and an encoding function

$$\epsilon_j^{\mathbf{x}}(\mathbf{r}) = e^{2\pi\sqrt{-1}\mathbf{x}\cdot\mathbf{r}}\overline{c_j(\mathbf{r})},$$
(1)

where c_j is the j^{th} coil sensitivity map and ${\bf r}$ is a spatial coordinate. Let $K_j^{\bf x}=F\epsilon_j^{\bf x}$ be the equivalent k-space sampling function and $M(S_A,S_B)$ be the $|S_A|\times |S_B|$ kernel matrix whose entries

$$M_{a,b} = \langle K_{j_a}^{\mathbf{x}_a}, K_{j_b}^{\mathbf{x}_b} \rangle \tag{2}$$

are inner products between Fourier-domain encoding functions corresponding to samples in either of the ordered sets S_A and S_B , where a and b index their respective sets. Each such entry equals the Fourier entry $F\{c_{j_a}\overline{c_{j_b}}\}(\mathbf{x}_a-\mathbf{x}_b)$. Then the RKHS interpolation weights from S_A to S_B are given by

$$W(S_A, S_B) = M(S_A, S_A)^{\dagger} M(S_A, S_B),$$
 (3)

where $(\cdot)^{\dagger}$ indicates the pseudoinverse. RKHS-based reconstruction is optimal in that it has maximum dimension, producing new weights for all data points for each interpolated point, generalizing standard methods like GRAPPA [7].

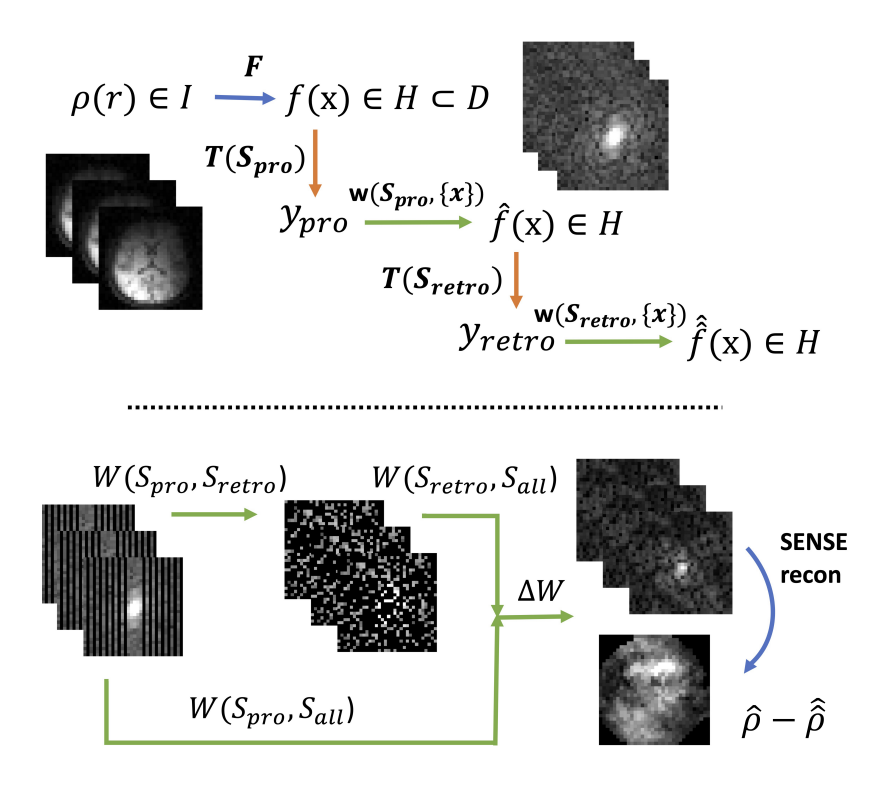


Fig. 3: Theoretical and computational framework. (a) $T(S_{\text{pro}})$ and $T(S_{\text{retro}})$ are discrete sampling operators, while elements of the RKHS H are continuous valued, such that $\mathbf{y}_{\text{pro}} = \{f_{j_p}(\mathbf{x}_p) | (j_p, \mathbf{x}_p) \in S_{\text{pro}}\}$ and $\mathbf{y}_{\text{retro}} = \{\hat{f}_{j_r}(\mathbf{x}_r) | (j_r, \mathbf{x}_r) \in S_{\text{retro}}\}$. (b) The PI data crime is then interpolation between three sets of coordinates. Interpolation weights for the experiment's error are the difference in weights for two reconstruction paths, one passing through S_{retro} and one skipping it.

2.2. Experiment Error Bound

Consider a linear retrospective experiment as illustrated in Figure 3. Reference data are prospectively acquired at points $S_{\rm pro}$ then reconstructed to a fully-sampled grid $S_{\rm all}$. Test reconstruction does the same after first interpolating to an intermediate pattern $S_{\rm retro}$. Observe that this chain of reconstructions is equivalent to direct interpolation between the subsets.

Denoting reconstructions \hat{f} and \hat{f} as in Figure 3, the error reported by the experiment on prospective data vector \mathbf{y}_{pro} can thus be directly interpolated by linear weights

$$(\hat{\hat{f}} - \hat{f})\Big|_{S_{all}} = \Delta W^{\top} \mathbf{y}_{\text{pro}},\tag{4}$$

where

$$\Delta W = W(S_{\text{pro}}, S_{\text{retro}}) W(S_{\text{retro}}, S_{\text{all}}) - W(S_{\text{pro}}, S_{\text{all}})$$
(5)

or some reduced-rank approximations of these matrices.

We next derive a data-independent error bound for retrospective experiment error. Let the multi-index $\mathbf{z}_a = (\mathbf{x}_a, j_a)$ contain both the k-space sampling coordinate and the coil index, and let $w(\mathbf{z}_a, \mathbf{z}_b)$ be the scalar interpolation entry $W(S_A, S_B)_{a,b}$. We are concerned with the power function of the difference in k-space between the prospective and retrospective reconstructions:

$$\left| (\hat{\hat{f}} - \hat{f})(\mathbf{z}) \right| = \left| \sum_{\mathbf{z}_r \in S_{\text{rates}}} \hat{f}(\mathbf{z}_r) w(\mathbf{z}_r, \mathbf{z}) - \hat{f}(\mathbf{z}) \right|$$
(6)

$$= \left| \sum_{\mathbf{z}_r} \sum_{\mathbf{z}_p \in S_{\text{pro}}} f(\mathbf{z}_p) w(\mathbf{z}_p, \mathbf{z}_r) w(\mathbf{z}_r, \mathbf{z}) - \sum_{\mathbf{z}_p \in S_{\text{pro}}} f(\mathbf{z}_p) w(\mathbf{z}_p, \mathbf{z}) \right|$$
(7)

$$= \left| \sum_{\mathbf{z}_p} \langle K^{\mathbf{z}_p}, f \rangle \sum_{\mathbf{z}_r} \left[w(\mathbf{z}_p, \mathbf{z}_r) w(\mathbf{z}_r, \mathbf{z}) - w(\mathbf{z}_p, \mathbf{z}) \right] \right|$$
(8)

$$= \left| \sum_{\mathbf{z}_p} \langle K^{\mathbf{z}_p} \Delta w(\mathbf{z}_p, \mathbf{z}), f \rangle \right| \tag{9}$$

$$\leq \|f\|_{H} \left\| \sum_{\mathbf{z}_{p}} K^{\mathbf{z}_{p}} \Delta w(\mathbf{z}_{p}, \mathbf{z}) \right\|. \tag{10}$$

Defining the normed term in (10) as the power function $p(\mathbf{z})$, the kernel's reproducing property gives the squared power,

$$p^{2}(\mathbf{z}) = \left\langle \sum_{\mathbf{z}_{p}} K^{\mathbf{z}_{p}} \Delta w(\mathbf{z}_{p}, \mathbf{z}), \sum_{\mathbf{z}_{p'}} K^{\mathbf{z}_{p'}} \Delta w(\mathbf{z}_{p'}, \mathbf{z}) \right\rangle$$
(11)

$$= \sum_{p \in S_{\text{Dro}}} \sum_{p' \in S_{\text{Dro}}} \langle K^{\mathbf{z}_p}, K^{\mathbf{z}_{p'}} \rangle \, \Delta w(\mathbf{z}_p, \mathbf{z}) \overline{\Delta w(\mathbf{z}_p', \mathbf{z})}. \tag{12}$$

In matrix form this simplifies to

$$\operatorname{diag}\left(\Delta W^{\top} M(S_{\text{pro}}, S_{\text{pro}}) \overline{\Delta W}\right). \tag{13}$$

This result, a point-wise upper bound, characterizes the structure and degree of error in the experiment. PI leverages linear consistency in the signal subspace spanned by the sensitivity maps [10]. This bound describes the relative difficulty of interpolating each point of k-space from the retrospective data versus direct interpolation from the prospective data. Its spatial structure depends on the prospective pattern, the retrospective pattern, and the sensitivity maps.

When $S_{\rm pro}=S_{\rm all}$, the power function describes the single-stage interpolation error of the retrospective experiment. Such a setting is "data-crime free" as all k-space points are Nyquist-rate samples of the data. On the other hand, when $S_{\rm pro}=S_{\rm retro}$, the retrospective experiment is trivial, requiring no new interpolation. This case maximizes the "data-crime", potentially (aside from possible regularization effects) suggesting an error-free result.

3. METHODS

Using the BART software toolbox [11], a 4-coil, 32×32 phantom was created in k-space so as to avoid an inverse crime [12]. We add noise to the data for an overall SNR of 35dB. Regularization set to 10^{-6} times the average eigenvalue of $M(S_{\rm all}, S_{\rm all})$ was added along the diagonal of all inverted matrices for all experiments. We apply the computational framework in Figure 3 to compare a few pattern combinations: a fully-sampled prospective grid versus an $R_{\rm pro}=2$ 2D uniform sampling pattern for an $R_{\rm retro}=3$ uniform 2D pattern; and an $R_{\rm pro}=4$ CAIPIRINHA [13] 3D prospective pattern versus an $R_{\rm pro}=4$ random 3D pattern for an $R_{\rm retro}=4$ random 3D pattern.

For each experiment, we show the SENSE reconstruction [7] after the chain of sampling, as well as the corresponding image and k-space errors. We also calculate and display the composite power function after interpolating to a full grid.

4. RESULTS

Figure 4 demonstrates the result of introducing a prospective 2D sampling pattern to a retrospective sampling experiment. An acceleration of $R_{\rm pro}=2$ is a standard clinical practice, and in fact, parallel imaging reconstructs missing k-space points effectively for a uniformly-spaced pattern. Still, the experiment power function, measuring interpolation difficulty between

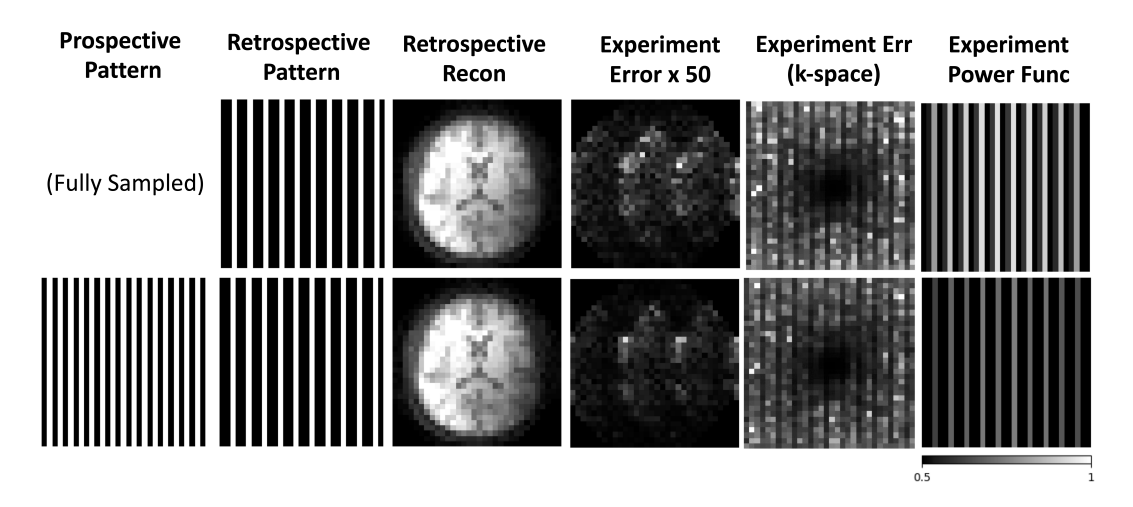


Fig. 4: Demonstration of direct interpolation of retrospective experiment error and power function calculation for 2D sampling patterns. Our analysis detects subtle changes in the image-domain error, as well as the magnitudes of the experiment power function when introducing this prospective pattern.

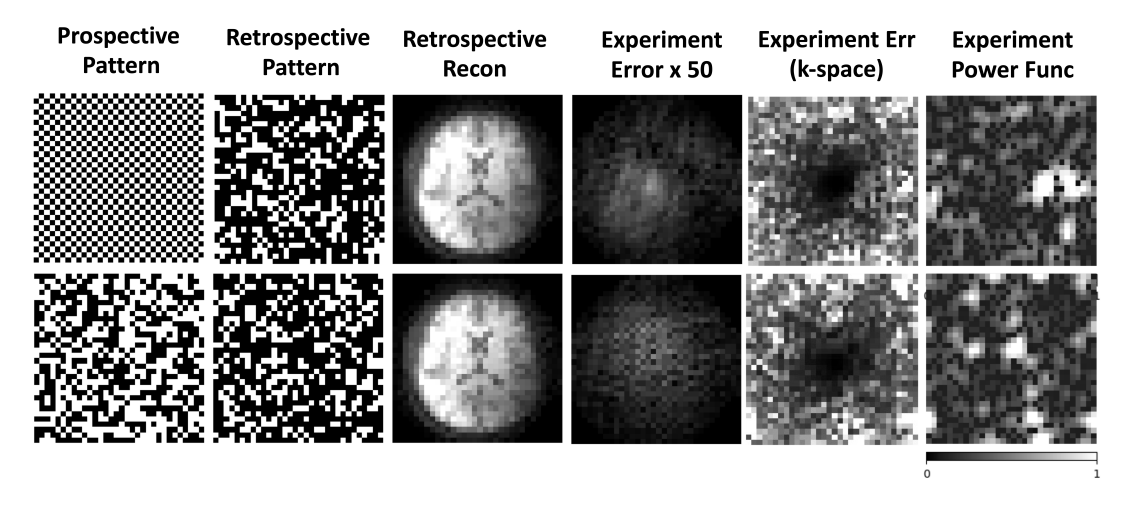


Fig. 5: Direct interpolation of retrospective experiment error and power function calculation for 3D sampling patterns.

this pattern and an $R_{\rm retro}=3$ uniform pattern along the same dimension, subtly but perceptibly is suppressed in magnitude compared to using a fully-sampled prospective dataset.

Figure 5 demonstrates combinations of 3D Cartesian sampling patterns, which might vary across two spatial dimensions. Interpolation to a random 3D pattern from a CAIPIRINHA grid generates a power function that is structured according to interpolation gaps in k-space. As this pattern minimizes gaps between k-space samples in 2D, it leads to a stable prospective reconstruction, such that the power function resembles the structure of the 3D pattern. A final example interpolates between two distinct random 3D patterns, outputting a power function that anticipates k-space error and contains structural features of both patterns.

5. DISCUSSION

Experiments visualize the connection between the power function derived above and the choice of sampling pattern pairs in the PI inverse crime. RKHS weights and their corresponding power functions are expensive to compute, requiring the solution to a linear system whose entries are $\Theta(N^2)$ in each dimension of the input data, and requiring up to $O(N^6)$ time to solve the system for an $N \times N$ image and even longer for 3D data. For this phantom case, however, RKHS theory successfully predicts the structure of retrospective experiment error for standard MR k-space sampling approaches.

Composite power functions give rigor to the related data crime phenomenon exhibited in [8]. The analysis is general and could be applied to arbitrary (e.g., non-Cartesian) sampling patterns. Upper bounds give useful information about the distribution of error in k-space, possibly aiding the design of future reconstruction regularizers and sampling pattern optimizers, as well as predicting the degree of bias due to use of sub-sampled data. While the high computational cost of RKHS interpolaters limits the immediate application of this work, there are clear connections to low-dimensional reconstructors such as GRAPPA and image-domain ones such as SENSE [7]. Subsequent analysis should attempt to bridge linear error analysis both to those methods and to non-linear AI-based reconstruction, helping researchers to improve the rigor of their algorithmic pipelines.

6. CONCLUSION

In conclusion, we presented a theoretical framework for analyzing implicit data crimes in multi-coil MRI arising from using PI-completed data for retrospective sub-sampling experiments. Our theory, based on RKHS, upper-bounds the error in linear reconstructors and could be used to detect and assess the degree of bias due to this implicit data crime.

7. COMPLIANCE WITH ETHICAL STANDARDS

This is a numerical simulation study for which no ethical approval was required.

8. ACKNOWLEDGEMENTS

Evan Frenklak is supported by NSF Award #2313998, subaward G-1B-022. This work was funded in part by grants from NSF CAREER CCF-2239687 Award, NSF IFML 2019844, and UT Joint Center for Computational Oncology Postdoctoral Fellowship.

9. REFERENCES

- [1] Chloe E. Hill, Evan L. Reynolds, James F. Burke, Moumita Banerjee, Kevin A. Kerber, Brandon Magliocco, Gregory J. Esper, Lesli E. Skolarus, and Brian C. Callaghan, "Increasing out-of-pocket costs for neurologic care for privately insured patients," *Neurology*, vol. 96, no. 3, pp. e322–e332, 2021, PMID: 33361253 PMCID: PMC7884984.
- [2] Reinhard Heckel, Mathews Jacob, Akshay Chaudhari, Or Perlman, and Efrat Shimron, "Deep learning for accelerated and robust mri reconstruction: a review," *Magnetic Resonance Materials in Physics, Biology and Medicine*, vol. 37, pp. 335–368, 2024, PMID: 39042206 PMCID: PMC11316714.
- [3] C. J. Kelly, A. Karthikesalingam, M. Suleyman, G. Corrado, and D. King, "Key challenges for delivering clinical impact with artificial intelligence," *BMC Medicine*, vol. 17, no. 1, pp. 195, 2019, PMID: 31665002 PMCID: PMC6821018.
- [4] Simen Sæmundsen Antun, Francesco Renna, Clarice Poon, Ben Adcock, and Anders C. Hansen, "On instabilities of deep learning in image reconstruction and the potential costs of AI," *Proceedings of the National Academy of Sciences*, vol. 117, no. 48, pp. 30088–30095, 2020, PMID: 32393633 PMCID: PMC7720232.
- [5] Junaid R. Rajput, Simon Weinmueller, Jonathan Endres, Peter Dawood, Florian Knoll, Andreas Maier, and Moritz Zaiss, "Death by retrospective undersampling – caveats and solutions for learning-based mri reconstructions," in *Medical Image Computing and Computer Assisted Intervention (MICCAI 2024)*. 2024, vol. LNCS 15007, pp. 233–241, Springer Nature Switzerland.
- [6] Efrat Shimron, Jonathan I. Tamir, Ke Wang, and Michael Lustig, "Implicit data crimes: Machine learning bias arising from misuse of public data," *Proceedings of the National Academy of Sciences*, vol. 119, no. 13, pp. e2117203119, 2022, PMID: 35312366 PMCID: PMC9060447.
- [7] Anagha Deshmane, Vikas Gulani, Mark A. Griswold, and Nicole Seiberlich, "Parallel mr imaging," *Journal of Magnetic Resonance Imaging*, vol. 36, no. 1, pp. 55–72, 2012, PMID: 22696125 PMCID: PMC4459721.
- [8] Evan Frenklak, Yamin Arefeen, and Jonathan I. Tamir, "Parallel imaging reconstruction in public datasets biases down-stream analysis in retrospective sampling studies," in *Proceedings of the International Society for Magnetic Resonance in Medicine*, 2024.

- [9] Vivek Athalye, Michael Lustig, and Martin Uecker, "Parallel magnetic resonance imaging as approximation in a reproducing kernel hilbert space," *Inverse Problems*, vol. 31, no. 4, pp. 045008, 2015, PMID: 25983363 PMCID: PMC4429804.
- [10] Justin P. Haldar and Kawin Setsompop, "Linear predictability in magnetic resonance imaging reconstruction: Leveraging shift-invariant fourier structure for faster and better imaging," *IEEE Signal Processing Magazine*, vol. 37, no. 1, pp. 69–82, 2020.
- [11] Martin Uecker et al., "The bart toolbox for computational magnetic resonance imaging," in *Proceedings of the International Society for Magnetic Resonance in Medicine*, 2016.
- [12] M. Guerquin-Kern, L. Lejeune, K. P. Pruessmann, and M. Unser, "Realistic analytical phantoms for parallel magnetic resonance imaging," *IEEE Transactions on Medical Imaging*, vol. 31, no. 3, pp. 626–636, 2012.
- [13] Felix A. Breuer, Martin Blaimer, Robin M. Heidemann, Matthias F. Mueller, Mark A. Griswold, and Peter M. Jakob, "Controlled aliasing in parallel imaging results in higher acceleration (CAIPIRINHA) for multi-slice imaging," *Magnetic Resonance in Medicine*, vol. 53, no. 3, pp. 684–691, 2005.